AIP | Journal of Applied Physics

Band alignment of epitaxial ZnS/Zn3P2 heterojunctions

Jeffrey P. Bosco, Steven B. Demers, Gregory M. Kimball, Nathan S. Lewis, and Harry A. Atwater

Citation: J. Appl. Phys. **112**, 093703 (2012); doi: 10.1063/1.4759280
View online: http://dx.doi.org/10.1063/1.4759280
View Table of Contents: http://jap.aip.org/resource/1/JAPIAU/v112/i9
Published by the American Institute of Physics.

Band alignment of epitaxial ZnS/Zn_3P_2 heterojunctions

Jeffrey P. Bosco,[a] Steven B. Demers, Gregory M. Kimball, Nathan S. Lewis, and Harry A. Atwater

Watson Laboratory and Noyes Laboratory, Beckman Institute and Kavli Nanoscience Institute, California Institute of Technology, 1200 E. California Blvd., Pasadena, California 91125, USA

(Received 10 September 2012; accepted 25 September 2012; published online 2 November 2012)

The energy-band alignment of epitaxial zb-ZnS(001)/α-Zn_3P_2(001) heterojunctions has been determined by measurement of shifts in the phosphorus 2*p* and sulfur 2*p* core-level binding energies for various thicknesses (0.6–2.2 nm) of ZnS grown by molecular beam epitaxy on Zn_3P_2. In addition, the position of the valence-band maximum for bulk ZnS and Zn_3P_2 films was estimated using density functional theory calculations of the valence-band density-of-states. The heterojunction was observed to be type I, with a valence-band offset, ΔE_V, of -1.19 ± 0.07 eV, which is significantly different from the type II alignment based on electron affinities that is predicted by Anderson theory. n^+-ZnS/p-Zn_3P_2 heterojunctions demonstrated open-circuit voltages of >750 mV, indicating passivation of the Zn_3P_2 surface due to the introduction of the ZnS overlayer. Carrier transport across the heterojunction devices was inhibited by the large conduction-band offset, which resulted in short-circuit current densities of $<0.1\ mA\ cm^{-2}$ under 1 Sun simulated illumination. Hence, constraints on the current density will likely limit the direct application of the ZnS/Zn_3P_2 heterojunction to photovoltaics, whereas metal-insulator-semiconductor structures that utilize an intrinsic ZnS insulating layer appear promising. © *2012 American Institute of Physics*. [http://dx.doi.org/10.1063/1.4759280]

Deployment of photovoltaics (PV) on the terawatt scale will require a low-cost, earth abundant, solar absorber with excellent optoelectronic properties. Zinc phosphide (α-Zn_3P_2) has a nearly optimal, direct band gap of 1.50 eV and a high visible-light absorption coefficient ($>10^4\ cm^{-1}$) near the band edge.[1,2] Zn_3P_2 has also been reported to have a long (>5 μm) minority-carrier diffusion length as well as passive grain boundaries.[3,4] These properties, in addition to the abundance of elemental zinc and phosphorus, make Zn_3P_2 promising for scalable thin-film photovoltaic applications.

The intrinsically p-type nature of Zn_3P_2 has led to a focus on Mg-Zn_3P_2 "Schottky" type photovoltaic cells, which have been reported to produce solar energy-conversion efficiencies of 6% and 4.3% for bulk and thin film devices, respectively.[3,5] The efficiency of these devices was limited by absorption and reflection from the Mg metal rectifying contact, by uncontrolled reaction/diffusion of the Mg into the Zn_3P_2 bulk,[6] and by a resulting high density of trap states at the Zn_3P_2 surface[7] which caused Fermi-level pinning in the device and hence produced low open-circuit voltages (V_{OC}). Heterojunction devices based on p-Zn_3P_2 absorbers include ZnO, Sn-doped In_2O_3 (ITO), CdS, or ZnSe as n-type emitters.[8–11] Heterojunction-based Zn_3P_2 devices have however exhibited relatively low V_{OC}'s, of ≤600 mV, and solar energy-conversion efficiencies of ≤2%. The low V_{OC} values can be attributed to poor band alignment between the emitter and the absorber layers and/or to inadequate interface passivation. Hence, fundamental studies of the band alignment of Zn_3P_2 with n-type semiconductor materials and the resulting impact that the band alignment may have on carrier transport, surface passivation, and device performance are important to the design of improved Zn_3P_2 heterojunction systems.

Desirable attributes of a heterojunction emitter partner for Zn_3P_2 include an n-type material that has a proper type I band alignment as well as a small conduction-band offset with Zn_3P_2. Zn_3P_2 has a low electron affinity (χ) of 3.6 eV,[12] and thus optimally requires a heterojunction partner that also has a low χ value. ZnS has a reported χ of 3.9 eV (Ref. 13) and is comprised of earth abundant elements. High levels of n-type doping in ZnS ($n > 1 \times 10^{19}\ cm^{-3}$) have been achieved through non-equilibrium growth techniques that enable the incorporation of extrinsic dopants comprised of either group III or group VII elements.[14–16] ZnS has also exhibited excellent surface passivation in heterojunctions with other semiconductors, including Si, Cu(In,Ga)Se_2, CdTe, and GaAs.[17–20] Anderson band alignment theory[21] predicts a valence-band offset (ΔE_V) and a conduction-band offset (ΔE_C) of roughly −2.5 eV and −0.3 eV, respectively, for a ZnS/Zn_3P_2 heterojunction. However, the actual band offsets often deviate from the ideal values,[22] thus highlighting the need for direct measurement of the energy-band alignment.

We report herein the energy-band alignment of zb-ZnS(001)/α-Zn_3P_2(001) heterojunctions grown by molecular beam epitaxy (MBE). The value of ΔE_V was determined using the method of Kraut *et al.* from high-resolution x-ray photoelectron spectroscopy (XPS) measurements according to[23]

$$\Delta E_V = \left(E_{CL}^{ZnS} - E_{VBM}^{ZnS}\right) - \left(E_{CL}^{ZnP} - E_{VBM}^{ZnP}\right) - \Delta E_{CL,i}, \quad (1)$$

where the first two components of Eq. (1) represent the core-level (CL) to valence-band maximum (VBM) energy

[a]Author to whom correspondence should be addressed. Electronic mail: jbosco@caltech.edu.

difference measured on the bulk ZnS and Zn_3P_2 surfaces, respectively. In this analysis, the S 2*p* and P 2*p* core-levels were used for ZnS and Zn_3P_2, respectively. $\Delta E_{CL,i}$ represents the energy difference between the S 2*p* and P 2*p* core-levels measured on an ultrathin ZnS/Zn_3P_2 heterojunction interface. From the value of ΔE_V, the corresponding value of ΔE_C was then calculated from the reported values for the band gaps of both of the materials that comprise the heterojunction of interest.

Compound-source epitaxy of Zn_3P_2 and ZnS was performed in an ultrahigh vacuum chamber with an ultimate pressure of $<2 \times 10^{-10}$ Torr.[16,24] Standard Knudsen effusion cells were used as compound sublimation sources for both Zn_3P_2 and ZnS. Epi-ready, Zn-doped ($>1 \times 10^{18}\,cm^{-3}$), p-type GaAs(001) single crystal wafers (AXT) were used as an epitaxial substrate. GaAs substrates of 1 cm^2 were mounted with In to a Cu chuck. The substrate was then degassed at 350 °C for 1 h in vacuum. The GaAs native oxide was removed at 450 °C by a ~5 min exposure to a RF-generated atomic hydrogen flux.[25] Film growths were performed at a substrate temperature of 200 °C. Thick films of Zn_3P_2 and ZnS (>150 nm), denoted as "bulk Zn_3P_2" and "bulk ZnS," were grown directly on the H-treated GaAs surfaces. The doping levels in the bulk films were $p \sim 1 \times 10^{15}\,cm^{-3}$ and $n \sim 1 \times 10^{17}\,cm^{-3}$ for Zn_3P_2 and ZnS, respectively. A series of ultrathin heterojunctions was fabricated by growth of a thick layer of Zn_3P_2 followed by growth of several monolayers of intrinsic ZnS. These structures are denoted herein by the ZnS film thickness. Hence a 0.6 nm ZnS film grown on Zn_3P_2 is denoted as 0.6 nm ZnS/Zn_3P_2.

XPS data of the P 2*p*, S 2*p*, and valence-band region (including the Zn 3*d* core-level) for each sample were obtained with monochromatic 1486.7 eV x-rays from a Kratos surface science instrument. Photoelectrons were collected at 0° from the surface normal with a detection linewidth of <0.26 eV. All spectra were processed using a "Shirley"-type baseline subtraction.[26] The P 2*p* region was fit using two doublet pairs that were modeled as 1:1 Gaussian-Lorentzian product functions. The first doublet represented bulk P–Zn bonding in Zn_3P_2 and the second, weaker doublet represented surface/interface P–P bonding (denoted as P^o). For both doublet pairs, the doublet area ratio was constrained to 2:1, and the doublet separation was constrained to 0.835 eV. The P^o $2p^{3/2}$ peak position was also constrained in the fitting process to 129.30 eV, based on a previous work on P-terminated Zn_3P_2.[27] The S 2*p* region was fit using a single doublet that was modeled with 1:1 Gaussian-Lorentzian product functions, with the doublet area ratio and peak separation constrained to 2:1 and 1.20 eV, respectively.

To accurately determine the position of the VBM in the measured spectra for the bulk ZnS and Zn_3P_2 samples, the valence-band region was fit with the valence-band density-of-states (VB-DOS) that was calculated for each material using *ab initio* density functional theory (DFT).[28] Calculations were performed within the Kohn-Sham framework and utilized the projector-augmented pseudopotentials as implemented in VASP.[29] Valence configurations of 3*d*4*s* were used for Zn and 3*s*3*p* for S and P with the Perdew, Burke, and Ernzerhof (PBE) potential.[30] Hybrid density functionals were also employed, thus addressing the "self-interaction error" and maintaining stronger electron localization. The VB-DOS was convoluted with an instrument-specific spectrometer response function, and was then fit to the leading edge of the valence-band region of the XPS data. The spectrometer response function was determined for the Kratos instrument by measurement of the Au 4*f* doublet, with the spectra fit to a Voigt function assuming an inherent Lorentzian linewidth of 0.317 eV and Gaussian broadening. The details of the convolution and fitting procedure have been outlined previously.[31]

To investigate the effect of the measured band alignment on the performance of heterojunction-based devices, current vs. voltage (*I-V*) measurements were performed under dark as well as simulated Air Mass (AM) 1.5 1-Sun illumination conditions on n^+-ZnS/p-Zn_3P_2 heterojunctions that were grown by molecular-beam epitaxy. The heterojunction was grown on a degenerately doped GaAs substrate ($p > 1 \times 10^{18}\,cm^{-3}$) with a Pt(20 nm)/Ti(30 nm)/Pt(10 nm) back contact. The degenerately doped GaAs was shown to make an ohmic contact to the Zn_3P_2 film. The ZnS and Zn_3P_2 film thicknesses were 120 nm and 1 μm, respectively, with nominal dopant densities of $n = 1 \times 10^{18}\,cm^{-3}$ and $p = 1 \times 10^{15}\,cm^{-3}$, respectively. The total junction area was ~0.35 cm^2, and an Al busbar with fingers was used as a top contact to the ZnS.

Fig. 1 displays reflection high-energy electron diffraction (RHEED) images of (a) a GaAs substrate that had been treated with atomic hydrogen; (b) a thick Zn_3P_2 epilayer surface; (c) a thick ZnS epilayer surface; and (d)-(f) thin ZnS/Zn_3P_2 heterostructures of various thicknesses. All RHEED images were collected with a beam energy of 20 keV that was incident along the GaAs[011] azimuth. The complete removal of the GaAs native oxide was evidenced by a streaky

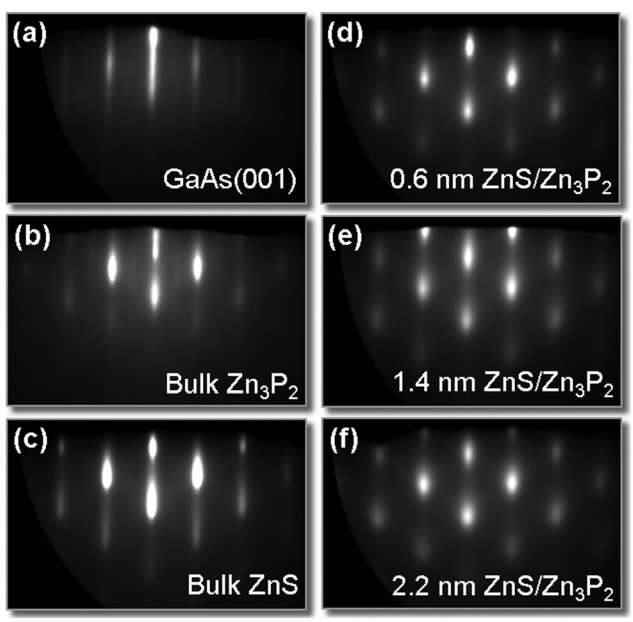

FIG. 1. *In situ* RHEED images of an (a) atomic hydrogen treated GaAs(001) surface, (b) 150 nm bulk Zn_3P_2 film, (c) 150 nm bulk ZnS film, (d) 0.6 nm ZnS/Zn_3P_2, (e) 1.4 nm ZnS/Zn_3P_2, and (f) 2.2 nm ZnS/Zn_3P_2. All RHEED images were obtained using a 20 keV electron beam incident along the [01$\bar{1}$] direction of the GaAs(001) surface.

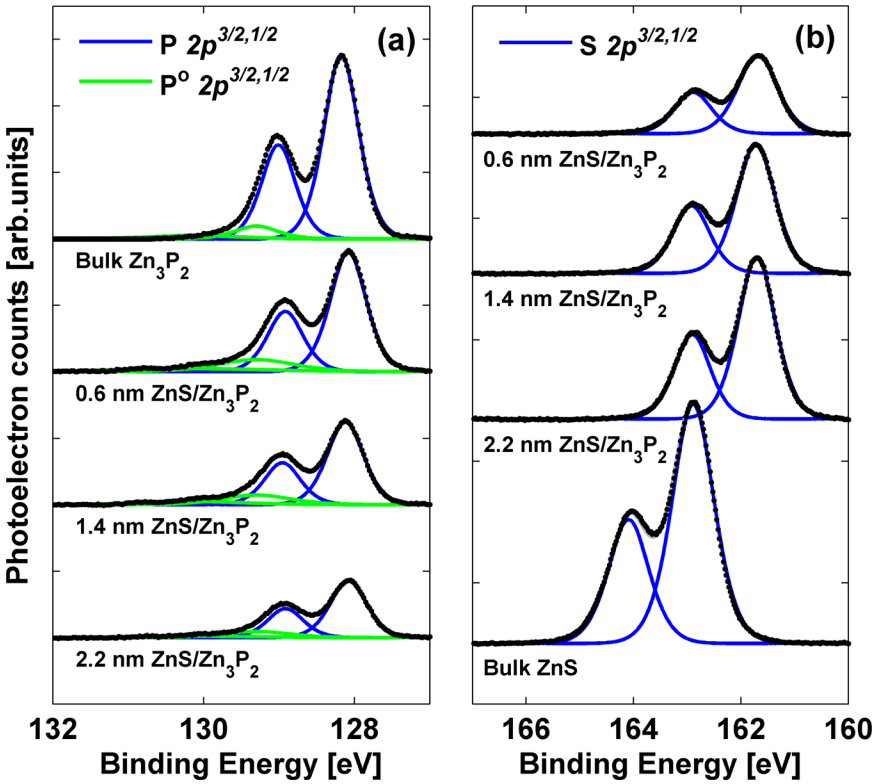

FIG. 2. X-ray photoelectron spectra of (a) P 2*p* and (b) S 2*p* core-levels for bulk Zn_3P_2, bulk ZnS, and several ultrathin ZnS/Zn_3P_2 heterojunction interfaces with different ZnS film thickness.

(1×1) surface reconstruction with the faint presence of a fourth-order reconstruction. The Zn_3P_2 grew in the tetragonal (α-phase) crystal structure along the (001) direction with a 45° in-plane rotation with respect to the GaAs lattice, as reported previously.[24] The Zn_3P_2 showed a streaky RHEED diffraction pattern, indicating that relatively smooth epitaxial films had been formed. A weak half-order reconstruction was also observed, which can be attributed to a Zn-terminated surface reconstruction. RHEED images of thick ZnS epilayers grown on Zn_3P_2 indicate that the ZnS structure was zinc-blende and that the ZnS grew in the (001) direction. The ultrathin ZnS layers were found to be slightly rougher than the thick layers, as indicated by spotty RHEED images. Relaxation of the ZnS lattice was considered complete upon initiation of growth, with no tetragonal strain observed in the RHEED images.

Fig. 2 displays the XPS data for the P 2*p* and S 2*p* core levels of bulk Zn_3P_2, bulk ZnS, and the 0.6 nm, 1.4 nm, and 2.2 nm ZnS/Zn_3P_2 heterojunctions. Oxide species were not observed in any of the core-level spectra. The fitted P $2p^{3/2}$ and S $2p^{3/2}$ core-level binding energies are reported in Table I. The 2*p* core-level position was taken as the mean of the fitted $2p^{3/2}$ and $2p^{1/2}$ peak positions for all of the following calculations. The spectra indicated a shift of ~1.2 eV in the S 2*p* binding energy upon formation of the heterojunction interface. However, little or no shift was observed for the P 2*p* binding energy. The core-level binding energy differences ($\Delta E_{CL,i}$) observed for all interface samples are displayed in Table I. An average value of $\Delta E_{CL,i} = 33.78 \pm 0.03$ eV was calculated for the five heterojunction samples.

Fig. 3 displays the XPS data obtained for the valence-band region of (a) bulk Zn_3P_2, (b) bulk ZnS, and (c) the

TABLE I. A complete list of P $2p^{3/2}$ and S $2p^{3/2}$ binding energies for all samples studied. Calculated E_{CL}-E_{VBM} for bulk samples and $\Delta E_{CL,i}$ and ΔE_V for heterojunction samples are also included. All values are reported in eV.

Sample	P $2p^{3/2}$	S $2p^{3/2}$	$\Delta E_{CL,i}$	$E_{CL} - E_{VBM}$	ΔE_V Kraut[a]	ΔE_V Direct[b]
Bulk Zn_3P_2	128.17(4)	…	…	128.46(9)	…	…
Bulk Zn_3P_2	128.13(6)	…	…	128.51(5)	…	…
0.6 nm ZnS/Zn_3P_2	128.08(2)	161.69(2)	33.79(2)	…	−1.20	−1.01
1.0 nm ZnS/Zn_3P_2	128.20(1)	161.79(3)	33.77(5)	…	−1.19	−1.15
1.4 nm ZnS/Zn_3P_2	128.12(0)	161.72(3)	33.78(5)	…	−1.20	−1.12
1.8 nm ZnS/Zn_3P_2	128.20(8)	161.76(2)	33.73(6)	…	−1.15	−1.18
2.2 nm ZnS/Zn_3P_2	128.07(9)	161.70(6)	33.80(9)	…	−1.22	−1.15
Bulk ZnS	…	162.89(1)	…	161.07(1)	…	…
Bulk ZnS	…	162.75(7)	…	161.08(7)	…	…

[a]Valence-band offset as calculated by the Kraut method using Eq. (1).
[b]Valence-band offset as determined by direct fitting of the interface valence-band spectra as a superposition of the bulk valence-band spectra.

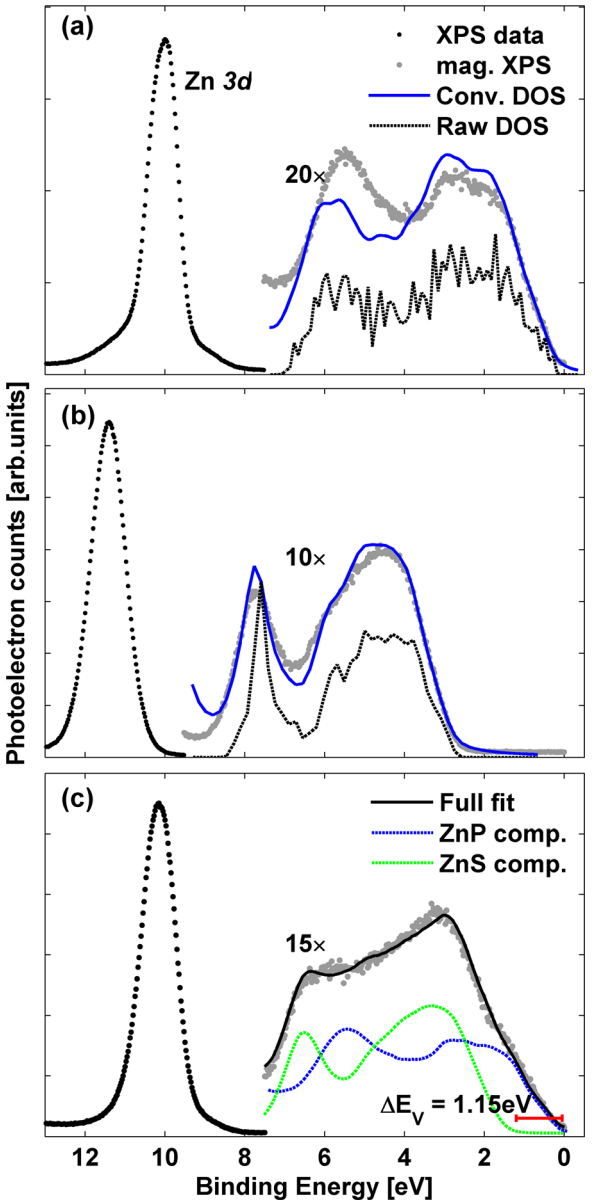

FIG. 3. XPS data of the valence-band region for (a) bulk Zn_3P_2, (b) bulk ZnS, and (c) a 1 nm ZnS/Zn_3P_2 heterojunction interface. For bulk samples, the raw and convoluted VB-DOS calculations that were used for determining the VBM are displayed. For the interface sample, the valence-band region was fit using a superposition of the bulk ZnS and bulk Zn_3P_2 valence-band spectra.

1.0 nm ZnS/Zn_3P_2 interface. For the bulk samples, the VB-DOS is also displayed as calculated (Raw DOS) as well as after convolution with the spectrometer response function (Conv. DOS). Excellent agreement was observed between the shape of the convoluted VB-DOS and the valence-band data collected by XPS. A ~0.24 eV difference was observed in the position of the ZnS VBM determined by the VB-DOS fitting relative to the value obtained using conventional linear extrapolation of the valence-band leading edge. The difference was likely due to a low calculated DOS near the edge of the valence-band. The low DOS was captured by the tail of the leading edge of the XPS spectra, which is not well represented by the linear extrapolation method, thus resulting in an overestimation of the VBM position. The core-level to VBM energy difference ($E_{CL} - E_{VBM}$) for bulk samples as determined by the VB-DOS fitting is listed in Table I. Average values for $E_{CL} - E_{VBM}$ of 128.49 ± 0.03 eV and 161.08 ± 0.01 eV were obtained for the bulk Zn_3P_2 and bulk ZnS samples, respectively.

From the core-level binding energies and VBM positions determined using the VB-DOS fitting, Eq. (1) yielded $\Delta E_V = -1.19 \pm 0.07$ eV. The ΔE_V was found to be independent of ZnS film thickness (see Table I), indicating minimal contributions due to any band bending near the interface. A direct determination of ΔE_V was also performed by fitting the measured valence-band spectra of a heterojunction interface to a superposition of the valence spectra of bulk ZnS and Zn_3P_2.[22] As displayed in Fig. 3(c) for the 1 nm ZnS/Zn_3P_2 sample, this process yielded excellent agreement between the fit and the XPS data. A value of ΔE_V was then directly calculated from the difference in the VBM positions of the superimposed bulk spectra. The fitted ΔE_V was similar across all heterojunction samples (see Table I) and resulted in an average $\Delta E_V = -1.12 \pm 0.07$ eV, which is consistent with the value of ΔE_V determined from Eq. (1). Use of the known band gaps for ZnS and Zn_3P_2 of 3.68 eV and 1.51 eV, respectively, yielded $\Delta E_C = 0.98 \pm 0.07$ eV.

The observed band alignment for the ZnS/Zn_3P_2 heterojunction interface differs significantly from the alignment predicted by Anderson theory (type I versus type II). Unlike devices comprised of III-V and II-VI compound semiconductors, the interfacial dipole that is expected to occur for the mixed II-VI/II-V heterojunction is currently not well elucidated. Ruan and Ching[32] proposed a simple theory for predicting deviations from Anderson theory based on interfacial dipole formation in the absence of interface defects. Their model predicts a decrease in the ΔE_V due to charge transfer from the higher valence-band material (in this case Zn_3P_2) to the lower valence-band material. Using their model, a ΔE_V between ZnS and Zn_3P_2 of -1.1 ± 0.1 eV is calculated, which is in excellent quantitative agreement with the experimentally measured offset.[34]

The measured electronic structure of the ZnS/Zn_3P_2 heterojunction may reflect effects of interfacial crystalline strain as well as interfacial chemical reactions. The *in situ* RHEED data indicated that the ZnS layers relaxed immediately upon film growth (see Fig. 1), implying that interfacial strain effects are minimal. Interfacial strain should also produce band offsets that depended on the thickness of the overlayer, in contrast to the experimental observations. Interfacial chemical reactions between P and S could produce deviations in the band alignment. Consistently, P–P bonding, or possibly P–S bonding, was observed in the XPS measurements of the ultrathin heterostructure samples. Attempts to limit reactions by exposing the Zn_3P_2 surface to a Zn metal flux immediately prior to ZnS deposition had no detectable effect on the XPS measurements or on the observed band alignment.

Fig. 4 displays the calculated band alignment of the proposed n^+-ZnS/p-Zn_3P_2 heterojunction under equilibrium conditions. The energy-bands were simulated using the AFORS-HET[33] device modeling software package, assuming $\Delta E_V = -1.19$ eV and realistic doping levels of

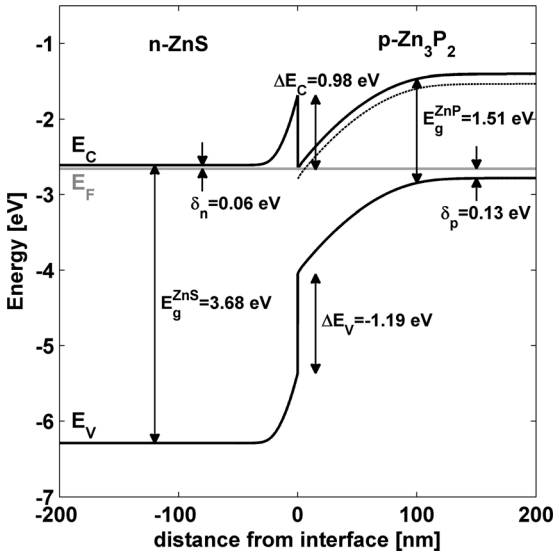

FIG. 4. The energy-band alignment for a ZnS/Zn_3P_2 heterojunction interface that was calculated given the experimentally measured ΔE_V and given the assumed doping levels of $n = 1 \times 10^{18}\,cm^{-3}$ and $p = 1 \times 10^{17}\,cm^{-3}$ for ZnS and Zn_3P_2, respectively. The dotted line below the conduction-band of Zn_3P_2 represents the indirect band gap of 1.38 eV.[2]

$n = 1 \times 10^{18}\,cm^{-3}$ and $p = 1 \times 10^{17}\,cm^{-3}$ for the ZnS and Zn_3P_2, respectively. The simulations demonstrated the existence of a large conduction-band spike at the ZnS/Zn_3P_2 interface due to the measured band offset. The conduction-band spike was found to inhibit charge transfer at the heterojunction interface and indicates that ZnS is a non-optimal emitter layer for Zn_3P_2. I-V measurements performed on n^+-ZnS/p-Zn_3P_2 heterojunctions confirmed this notion (Fig. 5), exhibiting short-circuit current densities of $<0.1\,mA\,cm^{-2}$ under simulated AM1.5 1-Sun illumination. However, the devices consistently demonstrated V_{OC}'s of >750 mV, indicating improved interface passivation over previously fabricated heterojunctions implementing Zn_3P_2 as an absorber layer. These results suggest that ZnS can provide a good surface passivation layer for Zn_3P_2 and may be useful as a thin, intrinsic layer in metal-insulator-semiconductor (MIS) or semiconductor-insulator-semiconductor (SIS) photovoltaic devices.

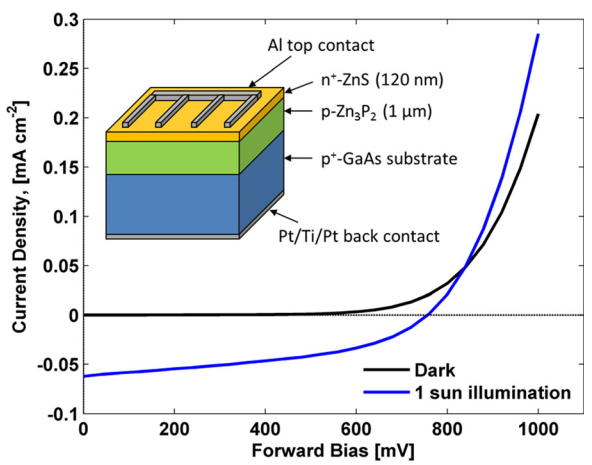

FIG. 5. I-V measurements for an MBE grown n^+-ZnS/p-Zn_3P_2/p^+-GaAs heterojunction device under dark and AM1.5 1-Sun illumination conditions. A schematic of the device is shown in the inset.

ACKNOWLEDGMENTS

This work was supported by the Dow Chemical Company and by the Department of Energy, Office of Basic Energy Sciences under Grant No. DE-FG02-03ER15483. The authors would like to thank Joseph Beardslee for his assistance with the Kratos XPS measurements. J.P.B. acknowledges the NSF for a graduate research fellowship.

[1]J. M. Pawlikowski, Phys. Rev. B **26**, 4711 (1982).
[2]G. M. Kimball, A. M. Müller, N. S. Lewis, and H. A. Atwater, Appl. Phys. Lett. **95**, 112103 (2009).
[3]M. Bhushan and A. Catalano, Appl. Phys. Lett. **38**, 39 (1981).
[4]K. W. Mitchell, Annu. Rev. Mater. Sci. **12**, 401 (1982).
[5]M. Bhushan, Appl. Phys. Lett. **40**, 51 (1982).
[6]L. L. Kazmerski, P. J. Ireland, and A. Catalano, J. Vac. Sci. Technol. **18**, 368 (1981).
[7]M. S. Casey, A. L. Fahrenbruch, and R. H. Bube, J. Appl. Phys. **61**, 2941 (1987).
[8]P. S. Nayar and A. Catalano, Appl. Phys. Lett. **39**, 105 (1981).
[9]T. Suda, M. Suzuki, and S. Kurita, Jpn. J. Appl. Phys., Part 2 **22**, L656 (1983).
[10]T. Suda, A. Kuroyanagi, and S. Kurita, in *Technical Digest, International PVSEC-1, Kobe, Japan* (PVSEC, Tokyo, 1984), p. 381.
[11]K. Kakishita, K. Aihara, and T. Suda, Sol. Energy Mater. Sol. Cells **35**, 333 (1994).
[12]A. J. Nelson, L. L. Kazmerski, M. Engelhardt, and H. Hochst, J. Appl. Phys. **67**, 1393 (1990).
[13]R. K. Swank, Phys. Rev. **153**, 844 (1967).
[14]M. Kitagawa, Y. Tomomura, A. Suzuki, and S. Nakajima, J. Cryst. Growth **95**, 509 (1989).
[15]S. Yamaga, A. Yoshikawa, and H. Kasai, J. Cryst. Growth **106**, 683 (1990).
[16]J. P. Bosco, S. F. Tajdar, and H. A. Atwater, "Molecular beam epitaxy of n-type ZnS: A wide-bandgap emitter for heterojunction PV devices," *Proc. 18th IEEE Photovol. Spec. Conf.*, Austin, June 3-8 2012 (IEEE, New York, 2012).
[17]G. A. Landis, J. J. Loferski, R. Beaulieu, P. A. Sekulamoise, S. M. Vernon, M. B. Spitzer, and C. J. Keavney, IEEE Trans. Electron Devices **37**, 372 (1990).
[18]Y. H. Kim, S. Y. An, J. Y. Lee, I. Kim, K. N. Oh, S. U. Kim, M. J. Park, and T. S. Lee, J. Appl. Phys. **85**, 7370 (1999).
[19]T. Nakada, M. Mizutani, Y. Hagiwara, and A. Kunioka, Sol. Energy Mater. Sol. Cells **67**, 255 (2001).
[20]J. M. Woodall, G. D. Pettit, T. Chappell, and H. J. Hovel, J. Vac. Sci. Technol. **16**, 1389 (1979).
[21]R. L. Anderson, Solid-State Electron. **5**, 341 (1962).
[22]A. Franciosi and C. G. VandeWalle, Surf. Sci. Rep. **25**, 1 (1996).
[23]E. A. Kraut, R. W. Grant, J. R. Waldrop, and S. P. Kowalczyk, Phys. Rev. Lett. **44**, 1620 (1980).
[24]J. P. Bosco, G. M. Kimball, N. S. Lewis, and H. A. Atwater, "Pseudomorphic growth and strain relaxation of α-Zn_3P_2 on GaAs(001) by molecular beam epitaxy," J. Cryst. Growth. (unpublished)
[25]A. Khatiri, J. M. Ripalda, T. J. Krzyzewski, G. R. Bell, C. F. McConville, and T. S. Jones, Surf. Sci. **548**, L1 (2004).
[26]D. A. Shirley, Phys. Rev. B **5**, 4709 (1972).
[27]G. M. Kimball, J. P. Bosco, A. M. Müller, S. F. Tajdar, B. S. Brunschwig, H. A. Atwater, and N. S. Lewis "Passivation of Zn_3P_2 substrates by aqueous chemical etching and air oxidation," J. Appl. Phys. (Communication) (to be published).
[28]S. Demers and A. van de Walle, Phys. Rev. B **85**, 195208 (2012).
[29]G. Kresse and J. Furthmüller, Comput. Mater. Sci. **6**, 15 (1996).
[30]J. P. Perdew, K. Burke, and M. Ernzerhof, Phys. Rev. Lett. **77**, 3865 (1996).
[31]E. A. Kraut, R. W. Grant, J. R. Waldrop, and S. P. Kowalczyk, Phys. Rev. B **28**, 1965 (1983).
[32]Y.-C. Ruan and W. Y. Ching, J. Appl. Phys. **62**, 2885 (1987).

[33]R. Stangl, M. Kriegel, S. Kirste, M. Schmidt, and W. Fuhs, in Proceedings of the IEEE Photovoltaic Specialists Conference, Orlando, FL, USA, 2005.

[34]See supplementary material at http://dx.doi.org/10.1063/1.4759280 for supplementary material includes: (1) XPS survey spectra for bulk and heterojunction samples; (2) the instrument response function fitting of the Au 4*f* core-level; (3) plots of the direct determination of the valence-band offset for all heterojunction samples; and (4) a detailed example of the valence-band offset calculation proposed by Ruan and Ching applied to the ZnS/Zn_3P_2 heterojunction.